Journal of Microscopy, Vol. 219, Pt 2 August 2005, pp. 76–85
Received 1 December 2003; accepted 30 May 2005

Reconstruction of pore space from a pore connectivity network via morphological transformations

L. L. TEO & B. S. DAYA SAGAR
Faculty of Engineering and Technology, Melaka Campus, Multimedia University, Jalan Ayer Keroh Lama, 75450 Melaka, Malaysia

Key words. Morphology, pore space, reconstruction, structuring element.

Summary

Pore and grain regions were separated via thresholding techniques from sandstone images. A mathematical morphology-based framework was followed to pack the random pore space with overlapping and nonoverlapping disks. This framework has several advantages in implementation and is generally applicable to multiscale images. The random pore space was reconstructed in two ways from the minimum morphological information through: (a) overlapping and (b) nonoverlapping disks of various shapes and sizes. The structuring elements employed to carry out this analysis included octagon, square and rhombus templates. The results achieved through these two types of reconstruction of sandstone pores are compared. These results provided the basis on which to test the accuracy of these techniques. Reconstruction recovery was tested by computing shapiness indices for the reconstructed pores achieved through the two methods.

Introduction

The reconstruction of random heterogeneous media, such as porous and composite media, from the knowledge of limited morphological information (Cule & Torquato, 1999) is an intriguing inverse problem. An effective reconstruction procedure enables one to generate accurate pore structures, and subsequently analysis can be performed on the image to obtain the desired macroscopic properties of the media. However, the structural quantities that are able to reproduce intrinsic two-dimensional (2-D) information, such as pore size distribution and the pore connectivity network need close examination (Lian *et al.*, 2004).

Another application includes the reconstruction of a three-dimensional (3-D) structure using information obtained from a 2-D image (Yeong & Torquato, 1998b). Yeong & Torquato (1998a) formulated a procedure to reconstruct the structure of general random heterogeneous media from limited morphological information by extending the methodology proposed by Rintoul & Torquato (1997). One of the systems created by Rintoul & Torquato (1997) is a random sequential adsorption process where nonoverlapping disks are placed randomly and sequentially on to a surface. Yeong & Torquato (1998a) also considered a variety of disks and Debye random media and a Fontainebleau sandstone samples were considered to show the results.

One can also probe the interesting issue of nonuniqueness, if limited microstructural information is given (Yeong & Torquato, 1998a). The aim of the reconstruction procedure is not just to reproduce an exact duplicate of the original image (Yeong & Torquato, 1998a). It is also to utilize the technique of packing based on random filling of the pore space with overlapping structuring templates of various sizes in order to reconstruct a pore space that has a similar morphological constitution. One of these inverse reconstruction methods was implemented by Radhakrishnan (2004). In the present investigation, we applied a procedure to identify the structuring element that was formed by applying an inverse process in the reconstruction of the image. This method is able to reproduce the pore space, providing a way to study the morphological characteristics.

The outline of this paper is as follows: first, we outline the basic morphological transformations used in the pore space reconstruction. Then we discuss how the morphological transformations are employed to reconstruct pores from the minimum morphological information by incorporating structuring elements in the random overlapping and nonoverlapping (Torquato, 2002; Radhakrishnan, 2004) reconstruction procedures. We also evaluate the results achieved from random packing in reconstruction, and compare them to the binary pore space of sandstone. We compare the structure pattern of the reconstructed pore image quantified using a shapiness index (Radhakrishnan, 2004). Finally, we provide conclusions and remarks.

Correspondence to: Lay Lian Teo. Tel: +60 62523850; fax: +60 6231 6552; e-mail: llteo@mmu.edu.my

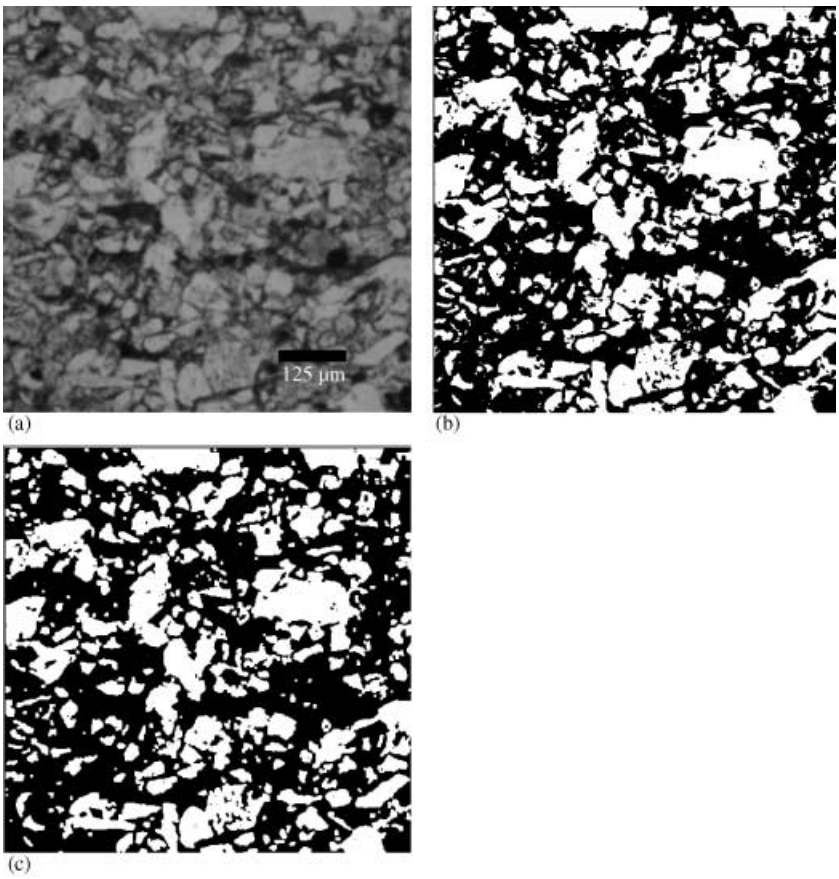

Fig. 1. (a) A slice of greyscale sandstone image acquired using a petrographic microscope. (b) Binary pore image of a sandstone image obtained via thresholding by specifying a grey level value of 128, and (c) the binary pore image after one cycle of opening. (Black and white colours, represent pore and grains, respectively.)

Morphological transformations

The discrete binary image, M (Fig. 1b), is defined as a finite subset of Euclidean 2-D space, Z^2 that can have the values 0 (grains) and 1 (pore). Morphological transformations are visualized as working with two images, namely the image being processed (M), and a structuring template (S) that possesses certain characteristic information such as shape, size, orientation, and origin. The pore image (M) can be decomposed by probing it with various structuring templates to unravel certain complex features of its topological nature. Let a digital binary pore M be represented by a set of elements $m \in M$. A morphological operation transforms M to a new image by a structuring element S. The four basic morphological transformations include *dilation* to enlarge, *erosion* to shrink, and *opening* and *closing* to smoothen are defined with respect to the structuring element S. These are represented in Eqs (1a–d) respectively.

$$\text{Dilation:} \quad M \oplus S = \{m+s : m \in M, s \in S\} = \bigcup_{s \in S} M_s \tag{1a}$$

$$\text{Erosion:} \quad (M \ominus S) = \{m-s : m \in M, s \in S\} = \bigcap_{s \in S} M_s \tag{1b}$$

$$\text{Opening:} \quad M \circ S = (M \ominus S) \oplus S \tag{1c}$$

$$\text{Closing:} \quad M \bullet S = (M \oplus S) \ominus S \tag{1d}$$

We purposefully omitted the basic information about these transformations, and the reader is encouraged to refer to Serra (1982) for more information. It is worth mentioning that the Minkowski's addition and subtraction are similar to morphological dilation and erosion as the considered structuring element $S = \hat{S}$, i.e. S is nothing but rotation by 180°. These transformations can be carried out according to a multiscale approach (Serra, 1982; Maragos, 1989) where the structuring element's size needs to be increased. In the multiscale transformations, cascades of erosion-dilation and dilation-erosion can be performed with respect to the structuring element S with scaling factor n. In this approach, the size of the structuring template increases from iteration to iteration as shown in Eq. (2).

$$S_n = \underbrace{S \oplus S \oplus S \oplus \ldots \oplus S}_{n \text{ times}} \tag{2}$$

The three types of structuring elements considered in the present investigation include rhombus, square and octagon. By performing these basic morphological transformations by means of three structuring elements, pore space is reconstructed by following overlapping and nonoverlapping procedures.

Overlapping and nonoverlapping reconstruction of pore image and accuracy verification via shapiness index

Sets of equations that are framed by following basic morphological transformations explained in the previous section are given to achieve reconstructed pore space through overlapping (Eq. 4) and nonoverlapping (Eq. 5) reconstruction procedures. Morphological reconstruction is the process of taking a partially connected component (skeleton points) and recreating the entire connected component (skeleton points), based on the intensities in the input image *M*.

In the present study, conversion of pore space into its pore connectivity network (PCN) was done by a simple skeletonization process (Serra, 1982; Sagar *et al.*, 2001). The *n-th* order *PCN* of a pore space (*M*), viewed as a subset of Z^2 (Euclidean discrete space), is defined as

$$PCN_n(M) = (M \ominus S_n) \backslash \{[(M \ominus S_n) \ominus S] \oplus S\} \quad n = 1, 2, \ldots, N \tag{3}$$

Using the PCN_n of several orders ranging from 0 to *n*, the union of which is termed minimum morphological information, the pore image is reconstructed by selectively dilating these connectivity network points with three structuring templates as shown mathematically below

$$D\text{-}PCN_n(M) = PCN_n(M) \oplus S_n \quad n = 1, 2, \ldots, N \tag{4a}$$

Dilated portions thus achieved are combined and form the overlapping reconstructed pore image ($RECON(O)$) as shown in Eq. (4b).

$$RECON(O) = \bigcup_{n=1}^{N} [PCN_n(M) \oplus S_n] \tag{4b}$$

However, the nonoverlapping pore image procedure is shown as Eq. (5) (Radhakrishnan, 2004).

$$\left.\begin{aligned} & M_2 = M_1 \backslash M_1 \circ S_n \\ & \quad \vdots \\ & M_n = M_{n-1} \backslash M_{n-1} \circ S_n \quad \text{and} \quad M_{n+1} = M_n \backslash M_n \circ S_n \\ & \quad \because \bigcup_{n=0}^{n} M_n = M \quad \text{and} \quad \because M_{n+1} = \phi \\ & RECON(NO) = M_{\text{Decomp}} \\ & \quad = (M \circ S_n) \cup (M_1 \circ S_n) \cup (M_2 \circ S_n) \cup \ldots \cup (M_{n-1} \circ S_n) \\ & \quad \because M_n \subset M_{n-1} \subset \ldots \subset M_3 \subset M_2 \subset M_1 \subset M \end{aligned}\right\} \tag{5}$$

In the interests of completeness, we briefly outline the method for the reconstruction using a nonoverlapping procedure, which is similar to that of random packing proposed previously (Manna & Herrmann, 1991; Dodds & Weitz, 2002). In this study, we consider the decomposition procedure that utilizes nonoverlapping structuring elements with sizes distributed from radius R_{max} to R_{min} in the *pore* image. Such a procedure decomposes the available *pore* space with the structuring elements of the higher radius (R_{max}). Once the pore image is decomposed into R_{max}, the procedure that reduces the radius of the structuring elements follows the procedure, and is repeated until R_{min} is reached. For a more detailed description of the general methodology, we refer to earlier work (Lian *et al.*, 2004).

In order to judge whether the pore space thus reconstructed through these overlapping and nonoverlapping procedures is appropriate, we compute the cumulative distribution functions of reconstructed and the original pore images as shown in Eq. (6).

$$\frac{A[RECON(M)]}{A[M]} = \frac{A\left[\bigcup_{n=1}^{N} [PCN_n(M) \oplus S_n]\right]}{A[M]} \tag{6}$$

In addition to this simple measurement, to appropriately understand the uniqueness of the reconstructed image, certain predefined structuring templates are employed to perform multiscale opening. The morphological opening transformation performed in the reconstruction of the pore image is represented in Eq. (7)

$$O - RECON(M) = \bigcup_{n=1}^{N} [PCN_n(M) \oplus S_n] \circ S_n \quad n = 1, 2, \ldots, N \tag{7}$$

Assuming that the reconstructed image has vanished after *n* cycles of multiscale opening, we estimate the area of resultant pore information after performing $(n-1)$ times of opening, $A[O - RECON(M) \circ S_{n-1}]$. The shapiness index (*SI*) is computed according to Eq. (8) for both original and pore images reconstructed via the overlapping and nonoverlapping procedures:

$$SI = A\left[\bigcup_{n=1}^{N} [PCN_n(M) \oplus S_n] \circ S_{n-1}\right] \Big/ A[RECON(M)] \tag{8}$$

where $A[RECON(M)]$ is the area of the reconstructed pore image. These results provided us with the necessary information to study the reconstruction accuracy.

Results and discussion

To demonstrate the application of mathematical morphologic transformations, we considered a thin section from a previous study (Lian *et al.*, 2004) shown in Fig. 1(a), which displayed pore features as black areas. Then the microscopic image was scanned by a video camera mounted to a microscope and was transformed into an array of digital granules. The pertophysical microscope image was obtained by scanning a television camera and transformed into an array of pixels with digital grey levels. The schematic flow for acquiring the image is as follows:

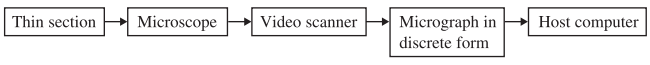

The pore structure from this image is isolated by simple thresholding techniques. In the present investigation, we made an attempt to study a morphologic aspect of pore structure isolated

from a single sandstone image sample acquired through a petrographic microscope fitted with a digital camera. This method could be adapted to a variety of petrographic problems and its use need not be restricted to the study of sandstone rocks.

A sandstone greyscale image of size 480×480 pixels (Fig. 1a) was used to perform the analysis. Pore space (Fig. 1b) was isolated by following a simple thresholding technique. The binary pore is opened by a rhombus of 3×3 size to filter out certain isolated minor patches. To achieve reconstruction of the pore space in a nonoverlapping way, morphological opening by reconstruction was further employed by means of three different structuring elements to understand the topologic properties of the pore space of sandstone. We employed the granulometric approach, in which multiscale morphologic opening is employed with respect to the rhombus structuring template. This opened pore image (Fig. 1c) is considered, and corresponding pore connectivity network subsets are extracted by following Eq. (3). Using the *PCN* subsets of several orders ranging from 0 to n, these subsets were dilated to the same degree and the combination of all these dilated versions produced the reconstructed pore images as explained in Eq. (4a–b).

For the first opening of image (M_1), we begin the reconstruction process at the skeleton points by choosing three different types of structuring elements such as the octagon, square 3×3 and rhombus for use in the reconstruction. The reconstruction using the nonoverlapping procedure was performed as

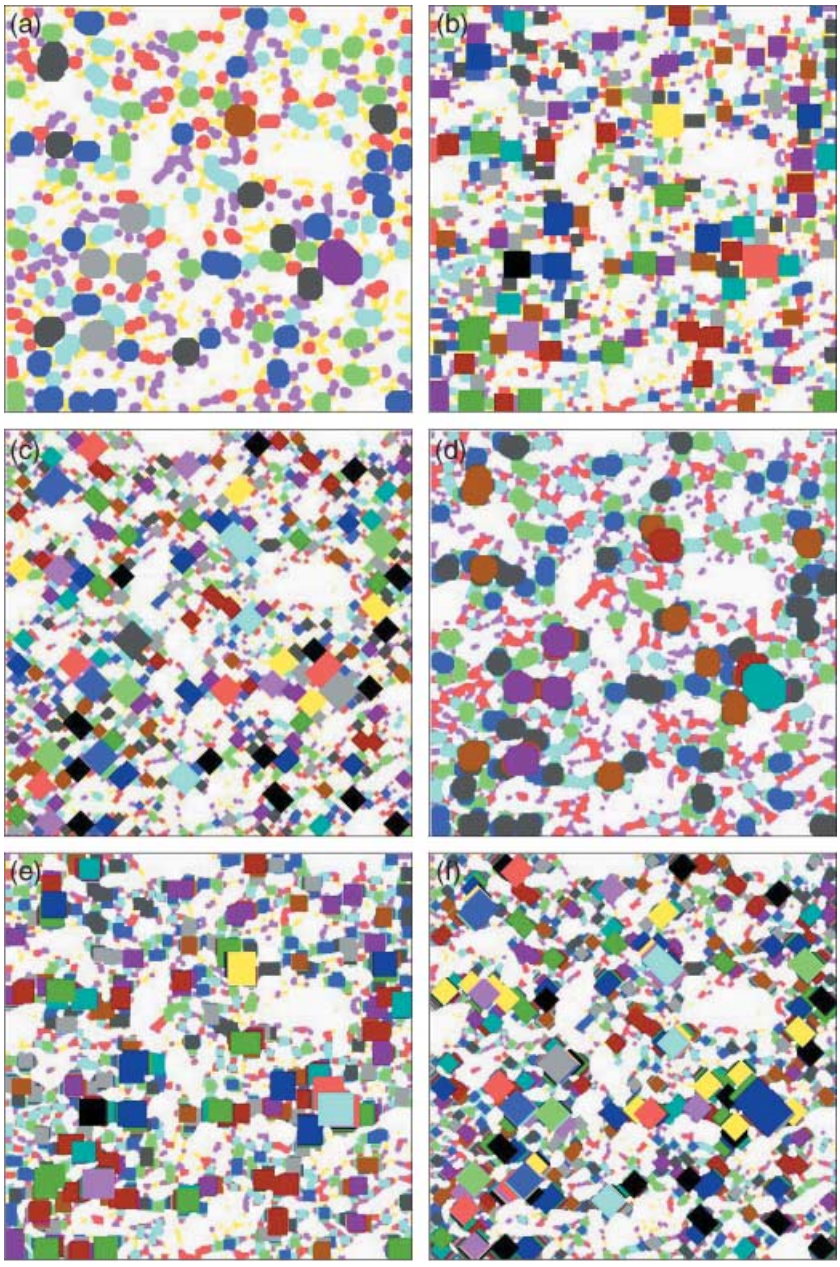

Fig. 2. Colour-coded reconstructed pore images. (a–c) Pore images reconstructed via the nonoverlapping procedure by means of octagon, square 3×3 and rhombus structuring elements, respectively. (d–f) Pore images reconstructed via the overlapping procedure by means of octagon, square 3×3 and rhombus structuring elements, respectively.

follows: we dilated skeleton points and combined these points to reconstruct the image. We illustrate the results using colour-coded reconstructed images with the three different structuring elements (Fig. 2d–f).

To observe the differences between the reconstructed images obtained by the overlapping and nonoverlapping procedures, we computed the nonoverlapping images by three structuring elements on the one-time opened image. To illustrate this decomposition of the pore with nonoverlapping structuring elements, we provide the results of colour coding of the reconstructed images achieved by considering octagon, square and rhombus templates (Fig. 2a–c). Nonuniqueness is expected due to the fact that the nonoverlapping packing generally does not provide morphological information (Fig. 2a–c). Incorporating overlapping structuring elements that are arranged in tight packing as shown in Figs 2(d)–(f) may produce a more refined reconstruction. In the reconstruction process, which is well documented (Torquato, 2002; fig. 12.19, p. 299), it is obvious that S_2-reconstruction, L-reconstruction and hybrid reconstruction S_2+L can be compared, respectively, with morphologic reconstruction via the overlapping and nonoverlapping procedures by means of the rhombus, square, and octagon (rhombus + square) templates. The basic difference between the reconstruction approaches employed in this study and in Torquato (2002) was the procedure used. The reconstruction approach we followed is based on morphological algorithms. Only approximated reconstruction was achieved in our study. This can be better comprehended from the data in Tables 1 and 2. To show the reconstruction accuracy, we derived shapiness indices. On the other hand, problems of showing the relationship between the shapiness indices, correlation function, and volume fractions still lies open.

Consequently, to judge the accuracy of the reconstruction, we measured and compared the important morphological measures and effective properties. The box counting method was performed on the original pore (Fig. 1c) and the threshold-reconstructed pore images (Fig. 3a–f). The cumulative distribution function by original pore area from reconstructed images to that of the original image is measured and shown in Table 1.

It may be misleading to compare the reconstructed space and the original image to validate the accuracy of the reconstruction. Note that the reconstructed pore with overlapping structuring elements closely resembles that of the pore space reconstructed by the nonoverlapping procedure. However, the reconstruction accuracy is observed better in the pore space that is reconstructed with nonoverlapping structuring elements. This is due to the fact that certain critical regions are not properly filled in the case of the pore that was reconstructed through the nonoverlapping structuring elements.

Smaller primitive structuring elements like the rhombus produce superior reconstruction, followed by the square 3×3 and octagon. However, from a practical point of view, it is important to realize that, if the structuring elements and effective overlapping properties of reconstruction agree closely with the reference image, the reconstruction by the overlapping procedure can be considered successful. It was observed that the reconstruction by the rhombus and square 3×3 accomplished the task accurately.

Additional microstructural measures were chosen for further comparison. We performed the opening (Figs 1c and 5a) of several cycles on the binary pore (Fig. 1b). We also chose the octagon, square 3×3, and rhombus structuring elements to reconstruct the pore (Figs 3d–f, 4a–c and 5b–d) to understand further the multiscaling properties of the pore reconstructed by nonoverlapping procedures. The cumulative distribution functions of the reconstructed images were compared with the original image (Table 2).

It is interesting to examine the accuracy of the reconstruction carried out by three different structuring elements. The reconstruction was most accurate for the pore space that was opened with four cycles. Furthermore, the pores reconstructed by smaller structuring elements such as the rhombus and square 3×3 match exactly when compared to that of the pore space reconstructed by octagons. The lower values of ratios reconstructed by the octagon (0.931, 0.948) indicate that the size of a primitive octagon is larger compared to a primitive rhombus and square 3×3, and it fails to fill in the actual pore system at critical regions. As expected, there are many areas in the pore where space is not filled with the octagon in a lower dimensional image. The reconstruction by these three structuring elements was found generally to underestimate all the measures that characterize morphological information of the pore space. However, octagons have a better capability to reconstruct the pore that is opened at a higher cycle number.

Table 1. Shapiness indices and ratios of areas between the original pore image and the pore image reconstructed via the overlapping and nonoverlapping procedures.

	Ratio of area of reconstructed pore image to original pore image			Ratio of shapiness index		
First time opening image	Octagon	Square 3×3	Rhombus	Octagon	Square 3×3	Rhombus
Overlapping reconstructed image	0.9484	0.9849	0.9873	0.0284	0.0119	0.0182
Nonoverlapping reconstructed image	0.8531	0.9315	0.9164	0.019241	0.012627	0.015318
Original image	1	1	1	0.016415	0.012085	0.018017

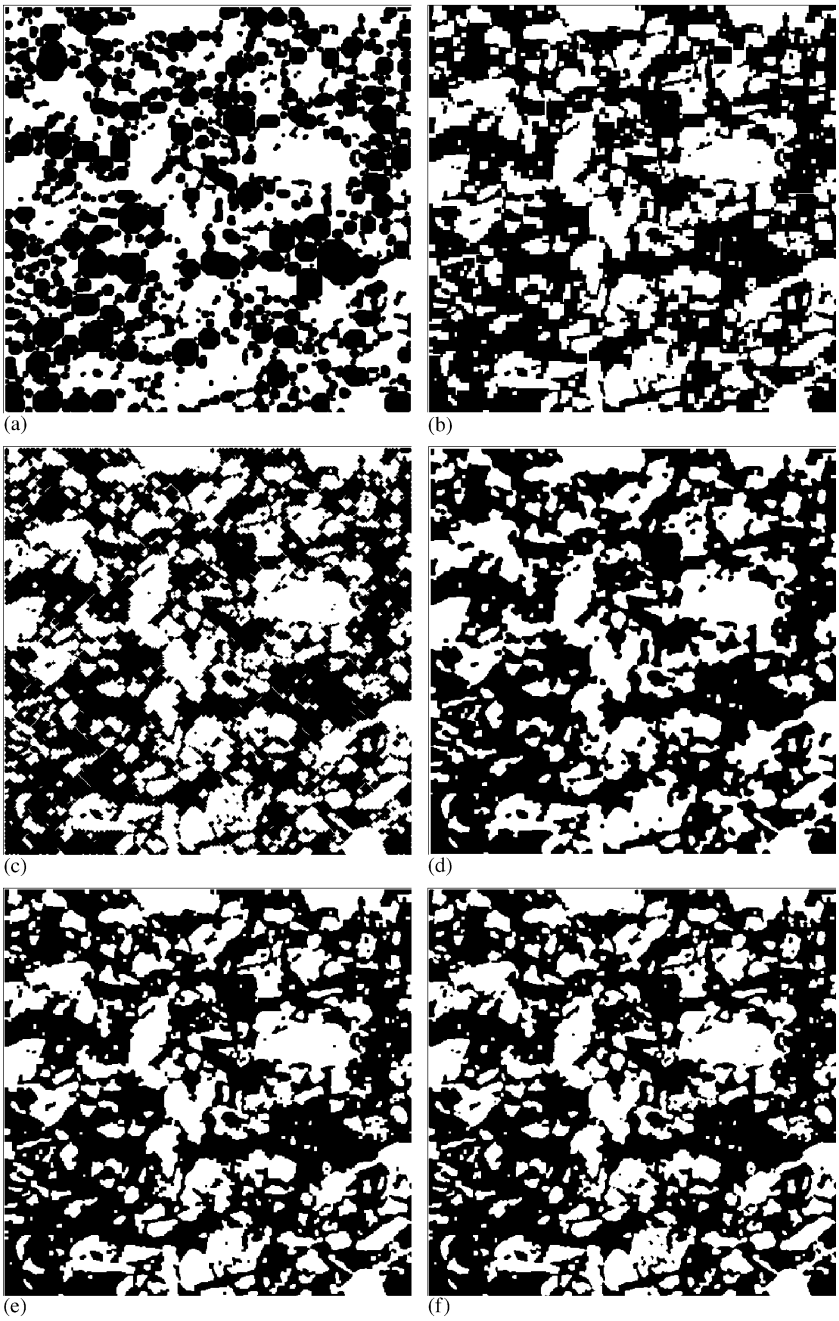

Fig. 3. Thresholded colour-coded pore images reconstructed (see Fig. 2) in binary form. (a–c) Binary pore images reconstructed via the nonoverlapping procedure by means of octagon, square 3×3, and rhombus structuring elements, respectively. (d–f) Binary pore images reconstructed via the overlapping procedure by means of octagon, square 3×3, and rhombus structuring elements, respectively. (Black and white colours, represent pore and grains, respectively.) The basic differences between these images (a–f) that look identical, are shown quantitatively in the first four columns of Table 1.

This may be due to the fact that the higher scaled pore space is smoothened to a greater degree, where the problem of a nonfilled critical region does not arise. Our explanation is that the small isolated pore spaces vanish due to the opening transformations applied in the pore space. The structuring elements of larger sizes are able to fill in a higher dimensional pore space. Again, as in the case of the rhombus, it gives the optimal matching in reconstruction. In general, pores reconstructed by structuring elements of larger sizes at lower pore space dimensions do not contain complete morphological information, and thus they cannot uniquely characterize the pore structure.

Consequently, to push the investigation on pore reconstruction even further, we investigated whether similar reconstruction can be achieved by different structuring elements if we apply the multiscale opening process on a reconstructed pore. Towards this goal, we provide an example of the opening process on the pore with nonoverlapping by octagon elements (Fig. 5). With the increasing number of iterations, random pores reconstructed by nonoverlapping octagon elements vanish from the smallest to largest sizes of octagon.

We show several realizations of the reproduction of morphological shapes or structuring elements at $N-1$ iterations before

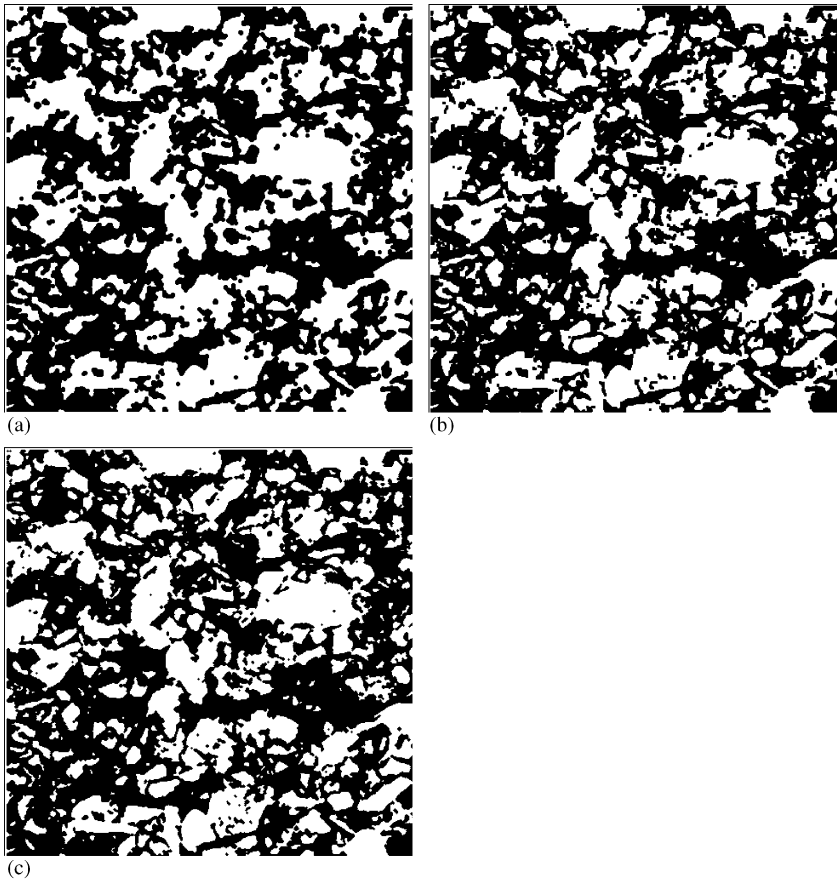

Fig. 4. (a–c) The reconstruction of the original binary pore image shown in Fig. 1(b), by using octagon, square 3×3, and rhombus structuring elements. For the quantitative results that illustrate the minor morphological variations in these seemingly identical images, refer to the first row of Table 2.

Table 2. Comparative analysis of estimated ratios between the areas of the original pore image and the images reconstructed via the overlapping procedure and shapiness indices.

The cycles of the opening process at original pore image	Ratio of area of reconstructed pore image to original pore image			Ratio of shapiness index		
	Octagon	Square 3×3	Rhombus	Octagon	Square 3×3	Rhombus
Original image	0.9316	0.9758	0.9835	0.01627	0.01198	0.01088
First time opening	0.9484	0.9849	0.9873	0.0284	0.0119	0.0182
Four times opening	0.9849	0.9883	0.9999	0.01840	0.01428	0.01294

the vanishing of the morphological shape for nonoverlapping (Fig. 6a–c) and overlapping (Fig. 6d–f) of the pore system. It was found that there are two octagon shapes retained after $N-1$ iterations (Fig. 6d). This implies that the reconstruction of the first time opening of the pore reconstructed through the overlapping procedure by the octagon occupied more space compared to that of the nonoverlapping while reconstruction.

This reconstruction of the pore space is commonly used to characterize its morphology. We chose to study these questions quantitatively by attempting to reproduce the morphological shapes by successfully reconstructing pore images. The shapiness index is computed to identify any physical phenomena of the structuring pattern formed by reproducing the structuring elements of reconstruction images. Shapiness indices computed for the reconstructed images with respect to different structuring elements are presented in Table 1. The reproduction of the octagon shapes in an overlapping reconstruction system is shown slightly better than for other reconstruction systems. We also found that there are no significant differences in the results obtained from choosing a square 3×3 (~0.12) or a rhombus (0.15–0.18). Graphical plots (Fig. 7) show that the area of the reconstructed pore decreases with an increasing number of iterations of the opening transformation. Different reconstructed systems contain distinctive morphological information. It was observed that the graphical plots obtained for the system reconstructed via the overlapping procedure are

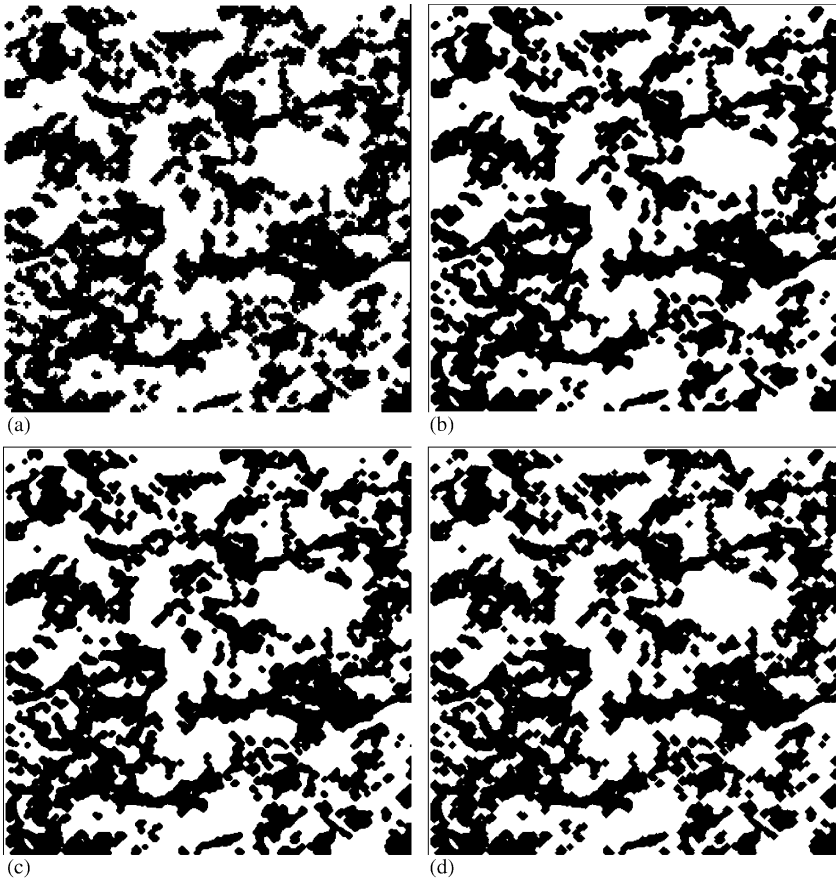

Fig. 5. (a) Pore image after four cycles of the opening transformation. (b–d) Reconstructed pore image after four cycles of opening through the overlapping procedure by means of octagon, square 3×3, and rhombus structuring elements, respectively. The third row in Table 2 may be referred to for the quantitative results that illustrate the basic morphological variations in these nearly identical images.

similar to those of the original system. However, the results of reproducing structuring elements at the nonoverlapping image are lower than the original system because it does not contain the complete morphological information at the reconstructed image.

Reproducing the morphological shape was successfully applied in the original and higher dimensional reconstructed systems and obtained the results of shapiness index in Table 2. The shapiness indices were computed for multiscale pore images that increased with increasing levels of multiscale.

Our explanation for this fact is that the smaller particles of microstructure in the higher dimension vanish due to the opening transformations with increasing size of the structuring element. The result of the shapiness index at higher dimensional pore images is shown. It is slightly higher than that for the original pore image. Therefore, the shapiness index is slightly higher due to the decreasing area of the pore systems.

We infer from the graphical plots (Fig. 8) that a decreasing trend occurs in the area at different multiscale dimensions of the reconstructed pore space. Different dimensions of reconstructed systems contain distinctive morphological information. It is also observed that the reconstructed pore area at the first time opening pore system is higher than those for the original system.

Conclusions

We employed morphological transformations to reconstruct the pore space by both overlapping and nonoverlapping procedures. This adopted framework is simple to implement and generally applicable to multidimensional pores. Furthermore, to judge the efficiency of reconstruction through overlapping and nonoverlapping procedures, we estimated the cumulative distribution function. The pore space reconstructed via the overlapping procedure matches closely to the original pore space as compared to the pore space reconstructed through the nonoverlapping procedure. However, the nonoverlapping reconstruction does not provide good results in reconstruction, which is due to the fact that many regions within the original pore space are not filled. The reconstruction by the three structuring elements was found generally to underestimate all the measures that characterize morphological information of the pore space. The reconstruction was done with more accuracy with the rhombus than with the octagon or the square. Larger structuring elements such as larger octagons failed to reconstruct the pore space accurately. However, the octagon-like templates were capable of filling in actual higher dimensional pore space.

Having obtained reasonably successful reconstruction results, we explored further information from the reconstructed pore

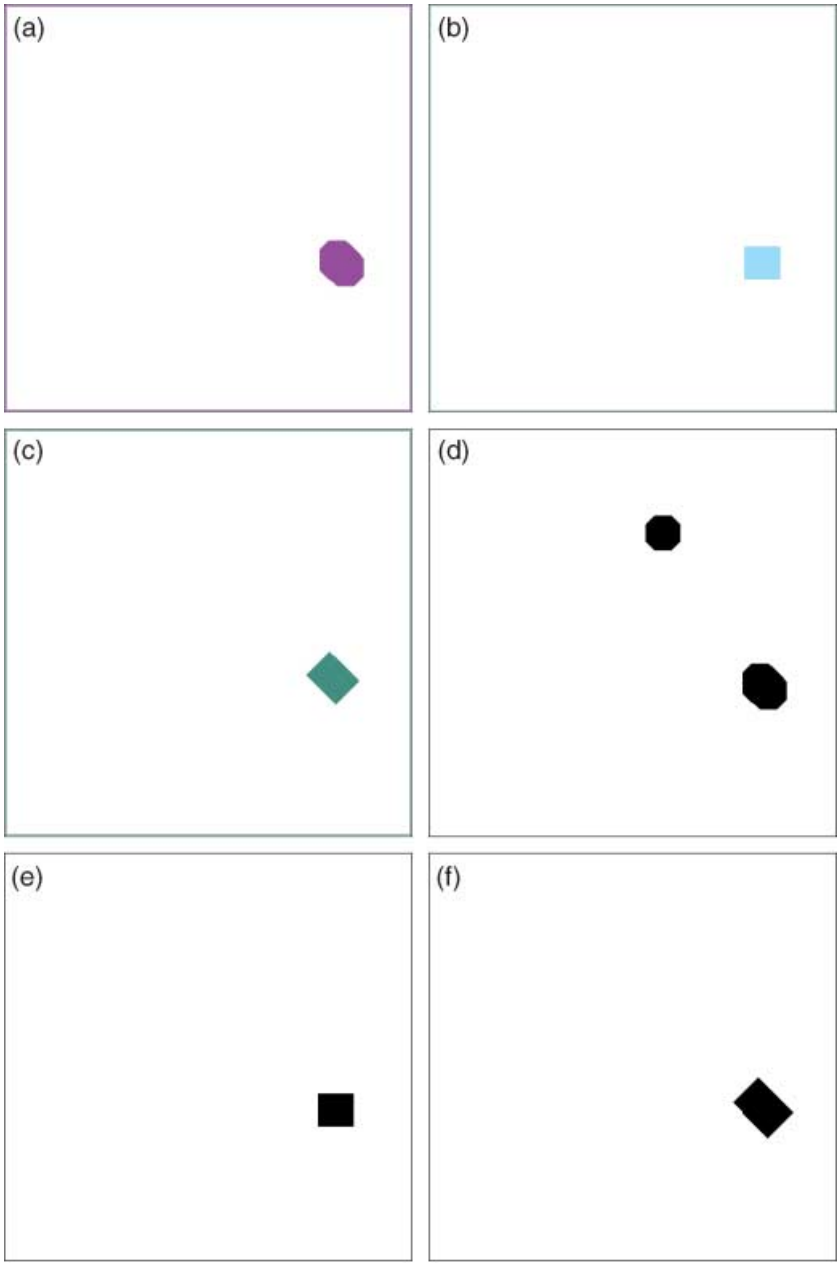

Fig. 6. (a–c) $N-1^{th}$ level portions of a pore obtained from a pore reconstructed via the nonoverlapping procedure by means of octagon, square, and rhombus structuring elements, respectively. (d–f) $N-1^{th}$ level portions of pores obtained from pores that were reconstructed via the overlapping procedure by means of octagon, square and, rhombus structuring elements, respectively. Note that images at the N^{th} level would yield empty sets.

space that relates to another intriguing inverse process in reconstruction, namely, shapiness index. The reproduction of the octagonal shapes in overlapping reconstruction was shown, which is better than other reconstruction at first time opening systems. This is due to the fact that morphological information obtained from reconstructed octagon images is incomplete.

We are currently extending our algorithm to address another intriguing problem, the reconstruction of 3-D pore structures from 2-D slices of MRI images, such as the extraction of brain from the human body, and schist from geological samples (provided by the University of Malaya). We will also compare the macroscopic properties of the referenced systems to the corresponding properties of the reconstructed systems. The results will be communicated in future publications.

Acknowledgements

The authors are thankful to P. Radhakrishnan for several discussions, Lim Tuck Meng and an anonymous reviewer for invaluable comments and suggestions. We gratefully acknowledge the support from the excellent computational facilities provided by Multimedia University, Malaysia. We are also thankful to M. Venu for providing a sandstone microphotograph.

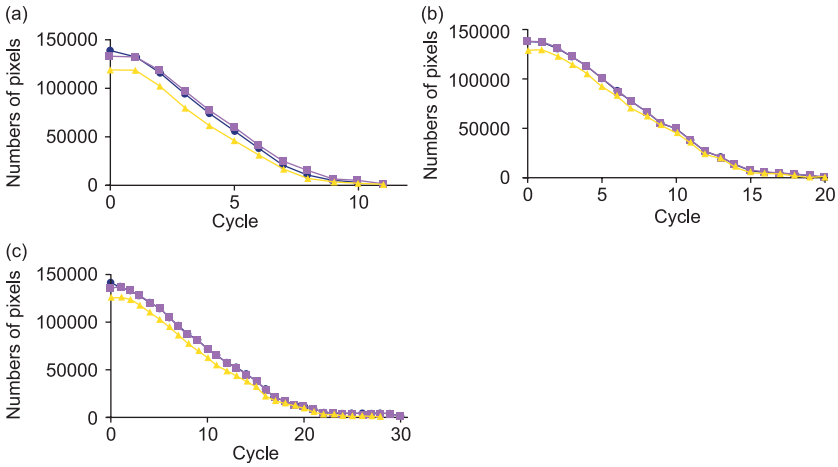

Fig. 7. Graphical plots between the opening cycle number and the corresponding areas of retained pore (in pixel units). Here, the input pore image considered was the original pore image (a–c) Areas of the original pore image and pore images reconstructed via the nonoverlapping and overlapping procedures, respectively, by means of octagon, square, and rhombus structuring elements are plotted as functions of the number of opening cycles. (Blue, yellow and pink colours in the plots represent, respectively, the original pore image and the pore images reconstructed via the nonoverlapping and overlapping procedures.)

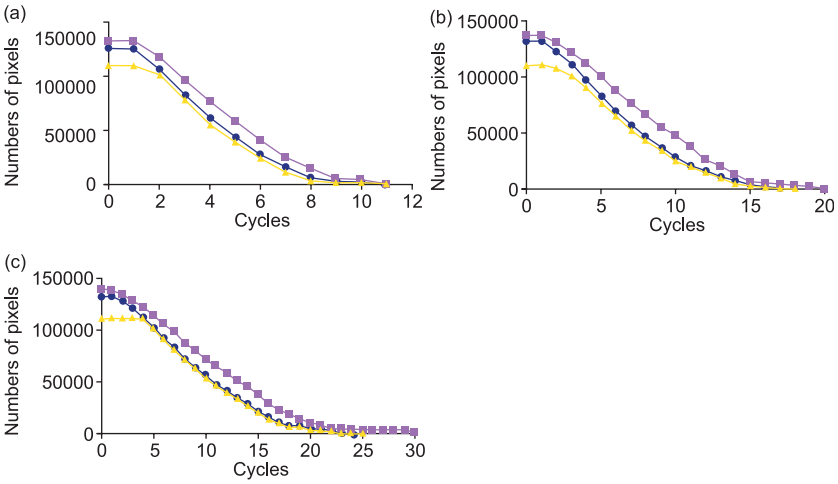

Fig. 8. Graphical plots between the opening cycle number and the corresponding areas of retained pore (in pixel units). The input pore image considered here was obtained after four cycles of opening. (a–c) Areas of multiscale pore image and pore images reconstructed via the nonoverlapping and overlapping procedures, respectively, by means of octagon, square, and rhombus structuring elements are plotted as functions of the number of opening cycles. (Blue, yellow and pink colours in the plots represent, respectively, the original pore image and the pore images reconstructed via the nonoverlapping and overlapping procedures.)

References

Cule, D. & Torquato, S. (1999) Generating random media from limited microstructural information via stochastic optimization. *J. Appl. Phys.* **86**, 3428–3437.

Dodds, P.S. & Weitz, J.S. (2002) Packing-limited growth. *Phys. Rev. E.* **65**, 056108.

Lian, T.L., Radhakrishnan, P. & Sagar, B.S.D. (2004) Morphological decomposition of sandstone pore space: fractal power-laws. *Chaos Solitons & Fractals*. **19** (2), 339–346.

Manna, S.S. & Herrmann, H.J. (1991) Precise determination of the fractal dimensions of Appollonian packing and space-filling bearings. *J. Phys. Math. Gen.* **24**, L481–L490.

Maragos, P. (1989) Pattern spectrum and multiscale shape representation. *IEEE Trans. Patt. Anal. Mach. Intel.* **11** (7), 701–716.

Radhakrishnan, P. (2004) *Discrete simulation, spatial modelling and characterisation of certain geophysical phenomena*. PhD Thesis, Multimedia University, Malaysia.

Rintoul, M.D. & Torquato, S. (1997) Reconstruction of structure of dispersions. *J. Colloid Interface Sci.* **186**, 467–476.

Sagar, B.S.D., Srinivas, D. & Rao, B.S.P. (2001) Fractal skeletal based channel networks in a triangular initiator basin. *Fractals*, **9** (4), 429–437.

Serra, J. (1982) *Image Analysis and Mathematical Morphology*. Academic Press, London.

Torquato, S. (2002) *Random Heterogeneous Materials: Microstructure and Macroscopic Properties*. Springer-Verlag, New York, pp. 252–254.

Yeong, C.L.Y. & Torquato, S. (1998a) Reconstructing random media. *Phys. Rev. E.* **57**, 495–506.

Yeong, C.L.Y. & Torquato, S. (1998b) Reconstructing random media II: Three-dimensional media from two-dimensional cuts. *Phys. Rev. E.* **58**, 224–233.